UNIVERSITY OF MINNESOTA
Driven to Discover℠

Suite 1000 ME
111 Church St. SE
Minneapolis, MN 55455-0111

Project Title: Embedded Nanocrystal Silicon Films: A New Paradigm for Improving the Stability of Thin-film Silicon

Contract Number: RD-3-25 **Milestone Number:** 10 **Report Date:** 9 June 2011

Principal Investigator: Uwe Kortshagen
612-625-4028

Contract Contact: Amy Rollinger
612-625-1359

Congressional District: (Corporate office) Minnesota 5th

Congressional District: (Project location) Minnesota 5th

MILESTONE REPORT

Executive Summary:

Under this grant, we pursue two different routes that may help increase the efficiency and lower the cost of thin film silicon solar cells. Our first approach (***Track 1***) is based on our unique ability to produce silicon nanocrystals in a low-pressure plasma-based synthesis reactor and to embed these nanocrystals in amorphous silicon films. Our novel deposition process enables us to independently control the properties of the amorphous matrix and of the crystalline phase, which we hope will enable us to improve the electronic quality of amorphous silicon that is used in thin film solar cells. In the second approach (***Track 2***), we study using such embedded nanocrystals as nuclei for seed-induced re-crystallization of amorphous silicon films. We expect that controlling the seed concentration will enable us to grow microcrystalline Si films faster and with grain sizes larger than possible with other deposition approaches. This may enable the cheaper production of solar cells based on microcrystalline silicon.

During the current project period, efforts under track 1 have focused on understanding the role of embedded nanocrystals in an n-type doped amorphous silicon film on the hydrogen motion in the films. A strong change of the hydrogen mobility is observed for crystal fractions exceeding 15%. We also observe a significant change in the conductivity relaxation with increased nanocrystal content in that films with higher crystal fraction show a conductivity that shows less relaxation over time. Infra-red absorption measurements suggest that hydrogen motion is impeded by clustering of hydrogen at the nanocrystal surfaces. The reduced hydrogen mobility with increased nanocrystal fraction appears to be beneficial for the stability of the films' electronic properties.

In track 2 we worked on introducing a generalized metric that would enable comparing the crystallization dynamics of our seeded films with microcrystalline films produced by other methods. We introduced the annealing factor as such a figure of merit. According to this metric, we find that crystallization kinetics of our nanocrystal seeded films is highly competitive with films crystallized by other methods. This demonstrates that our paradigm of nanocrystal seeding is a viable alternative compared to other solid phase crystallization methods.

Project funding provided by customers of Xcel Energy through a grant from the Renewable Development Fund.

Technical Progress:

Both tracks of the project have made good progress and achieved the milestone set in the contract. The progress made on both tracks will be discussed below.

Track 1: ***Embedded nanocrystals in amorphous silicon***

Within this research track, we are continuing to study the effects of the embedded silicon nanocrystals on the optical and electronic properties of hydrogenated amorphous silicon (a/nc-Si:H). This quarter we have investigated the hydrogen motion in n-type doped a/nc-Si:H thin films. A major limitation of hydrogenated amorphous silicon (a-Si:H) devices that limits them from fulfilling their technological potential, is the light-induced defect creation effect, also known as the Staebler-Wronksi effect. While the microscopic mechanism underlying the Staebler-Wronski effect in a-Si:H has not been definitively elucidated, most models posit that the motion of bonded hydrogen plays a central role in either the formation or stabilization of the light-induced defects. Hydrogen motion also influences the electronic properties of doped a-Si:H films even in the absence of light exposure, through "thermal equilibration" effects. The electronic properties of doped a-Si:H are found to be independent of thermal history above a kinetically determined "equilibration temperature" (often denoted T_E), and are characterized by a metastable equilibrium below T_E, displaying many of the characteristics of glasses, such as history dependent conductivities (whose values are sensitive to the cooling rate following annealing above T_E) and slow, stretched exponential relaxations [1,2]. Considerable evidence indicates that the motion of bonded hydrogen in doped a-Si:H underlies these glassy dynamics [2]. This report is a follow-up of the preliminary results described in quarterly report 8 (Q8).

The films used in this study were grown in a two-chamber co-deposition system, described in the first quarterly report (Q1), in which the nanoparticles are synthesized in a plasma reactor using silane (SiH_4), argon and phosphine (PH_3). The doping level was set at $[PH_3]/[SiH_4] = 6 \times 10^{-4}$ for all of the films studied here. The nanocrystallites are grown in the particle reactor chamber, which are then entrained by the argon and injected into a second PECVD chamber where a-Si:H is deposited using the residual silane/dopant gas mixture from the first chamber. The films reported here have crystalline contents ranging from < 1% to 29%, as determined by Raman spectroscopy measurements described below. The low temperature electronic properties of these films were reported in the previous quarterly report (Q9).

The crystalline content of the a/nc-Si:H films is analyzed via Raman spectroscopy, using a Witec Alpha 300R confocal Raman microscope, equipped with an UHTS 200 spectrometer and an argon ion excitation laser of wavelength 514.5 nm at a power of 5 mW focused to an area of ~ 2-3 μm diameter. The crystal fraction is quantified using the typical formula:

$$X_C = \frac{I_{520} + I_{500}}{I_{520} + I_{500} + I_{480}} \qquad (1)$$

Here, I_{480} and I_{520} represent the areas under the amorphous (480 cm^{-1}) and crystalline (520 cm^{-1}) TO peaks respectively, indicated in Fig. 1a. The nanocrystalline TO mode, while near 520 cm^{-1}, is typically shifted by several wavenumbers, due to a variety of effects, including quantum confinement, stress, and surface states of the nanocrystals.

The hydrogen bonding in these mixed-phase films is characterized by Fourier transform infrared spectroscopy (FTIR) using a Nicolet Magna 750 Fourier Transform Infra-Red (FTIR) spectrometer. The infra-red absorption for wavenumbers near 2000 cm^{-1} results from excitation of the Si-H stretching mode. Often two distinct peaks can be observed in the FTIR spectrum, indicating differing local environments of the Si-H bonds. While the peak at 2000 cm^{-1} is ascribed to the isolated Si-H stretch mode, the mode at 2090 cm^{-1} has been attributed to either the presence of Si-H_2 modes or clustered Si-H modes. A sample plot for films grown in our deposition system can be seen in figure 1b. As X_C is increased, an increase of the absorption of the 2090 cm^{-1} peak relative to the 2000 cm^{-1} peak is observed, which is often associated with higher amounts of structural disorder in the film.

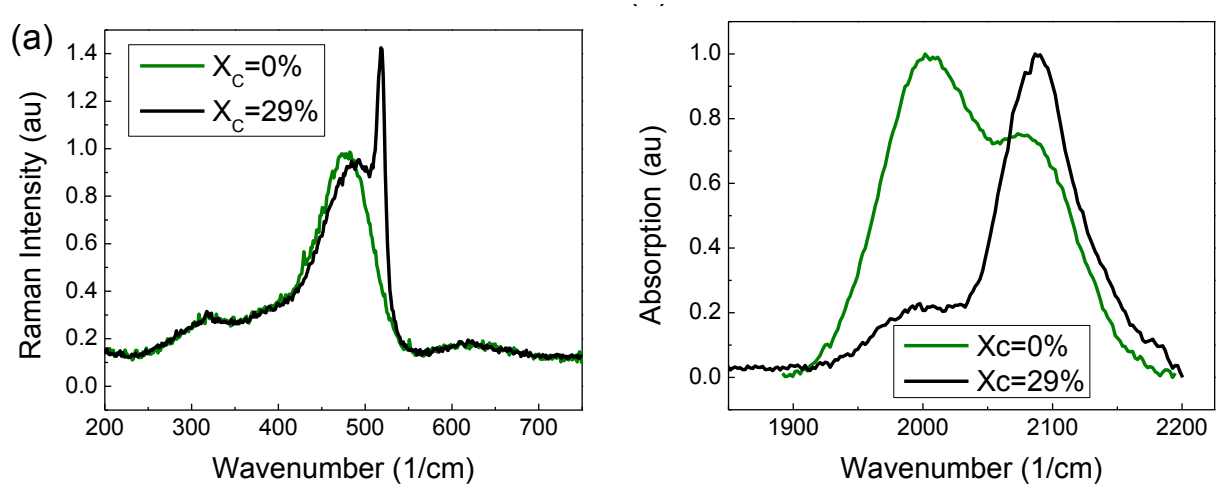

Figure 1: Raman spectrum (a) and Fourier Transform Infra-red Absorption Spectrum (b) for doped a-Si:H with no nanocrystalline inclusions (X_C = 0%, green/gray) and for a crystalline content of X_C = 29% (black). The data is normalized to the baseline of the amorphous TA, LO and LA peaks (a) or the absorption at 1900 cm^{-1} (b).

To measure and quantify the thermal equilibration properties of the electronic transport in the n-type doped a/nc-Si:H films, the temperature dependence of the conductivity is measured as a function of quench-rate from a high temperature anneal. In addition, the slow, time-dependent relaxation of the conductivity at a single temperature below the equilibration temperature is recorded. The former is identical to tests used by Kakalios and Street [1], while the latter are equivalent to sweep-out measurements described in Kakalios *et al* [2].

For the conductivity measurements, the films were annealed at 470K for 30 min and then quenched to room temperature at varying cooling rates, ranging from 0.1K/min to 100K/min. The conductivity of the film was then measured under vacuum in the dark upon warming at a constant rate of 1K/min. For a conventional, doped a-Si:H film with no nanocrystalline inclusions, below T_E (~400K) the conductivity magnitude and activation energy is sensitive to the rate at which the sample is cooled from the high temperature anneal, while above this temperature the conductivity is independent of thermal history [1]. In order to characterize the magnitude of the thermal equilibration effects, we define a "conductivity gap" as the ratio of the magnitude of the dark conductivity following a fast (100K/min) cool to that resulting from a slow (0.1 K/min) cool at a particular temperature. In the absence of any thermal equilibration effects, this ratio should

be unity, that is, the dark conductivity will be insensitive to the rate at which the film is cooled from a high temperature anneal. The results are plotted in figure 2. There is relatively little change in the "conductivity gap" for the low crystalline content films, followed by a dramatic decrease to values near unity for films with crystalline content in the 10 – 20% range. The data in figure 2 is for the dark conductivity measured at 350K, though the same trend is observed for other temperatures below 400K.

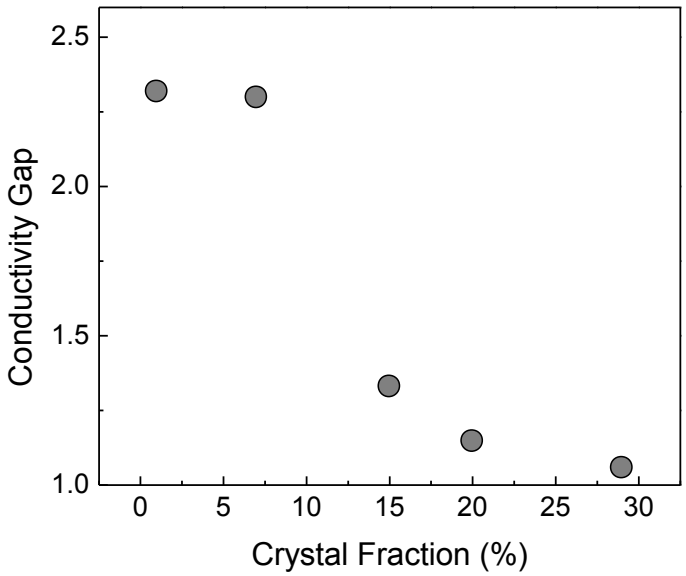

Figure 2: The conductivity gap, defined as the ratio of the dark conductivity at 350K measured after rapid quenching at 100 K/min from a high temperature anneal to the conductivity measured at the same temperature after slow cooling at 0.1 K/min cool, for varying crystal fractions.

For the relaxation measurements, the film was again annealed at 470K and then rapidly quenched at ~100K/min to slightly below the measurement temperature. The temperature was then stabilized at the measurement temperature and the conductivity was monitored as a function of time. For temperatures below the equilibration temperature, the conductivity slowly relaxes to a lower value. The relaxation curves are generally fit to a stretched exponential time dependence [2]:

$$\sigma = \sigma_0 \exp\left[-(t/\tau)^{\gamma}\right] \qquad (2)$$

Where τ is the relaxation time and the exponent is $\gamma < 1$. Assuming a time-independent mobility and using $\sigma = ne\mu$, this is a measurement of the carrier concentration as a function of time. The conductivity relaxation curves are plotted in figure 3 for the same films as in the previous conductivity plots (figure 2), measured at a fixed temperature of 410K. For mixed-phase films with a crystal fraction above 7%, the time for the conductivity to relax to a steady state value increases, and for the highest crystal fractions only an incomplete relaxation is recorded. Consequently for these films the current could not be normalized to both the initial and final values (as needed for a proper fit to a stretched exponential time dependence, precluding accurate determinations of

γ and τ). The data plotted in figure 3 is the current as a function of time, normalized to the current at an initial time of 1 sec.

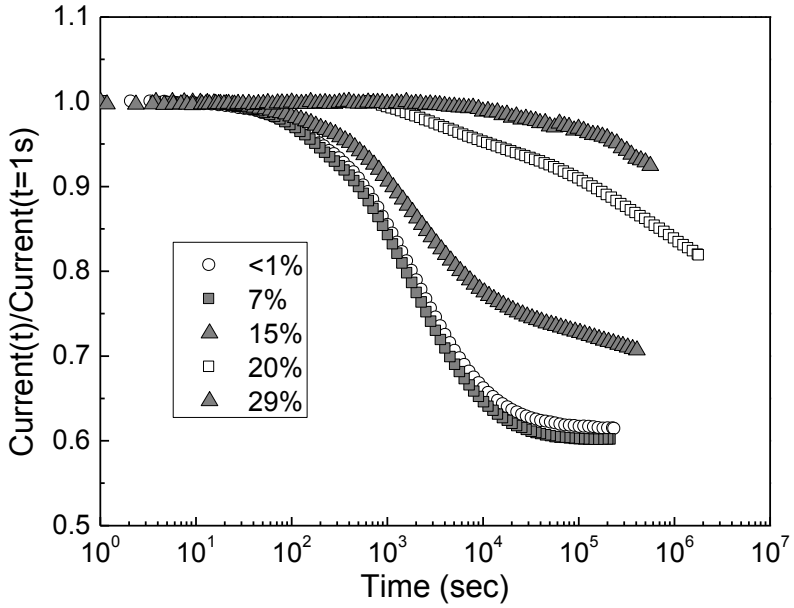

Figure 3: Conductivity relaxation plots at a fixed temperature (410K) for n-type doped a/nc-Si:H films with differing crystal fractions, showing the increase in relaxation time as the crystal fraction is increased. The curves have been normalized to the current recorded at t = 1 sec.

Slower H motion in mixed-phase films with higher crystal fractions, which would imply a reduction in the Staebler-Wronski effect, could be due to a phenomenon seen in films with large amounts of clustered hydrogen, where the hydrogen kinetics are slowed considerably due to trapping of the hydrogen in these clustered sites [3]. The increase in the amount of hydrogen in either the clustered phase or the Si-H_2 configuration as the crystal fraction increases is observed in the FTIR results (figure 1b). Previous studies of undoped a/nc-Si:H, produced in a similar fashion in a dual-chamber co-deposition system, found that the microstructure fraction increased with increasing crystalline content [4]. Comparisons of the increase in the FTIR absorption at 2090 cm^{-1}, compared to films with no nanocrystalline inclusions (produced under the same conditions, but with the particle reactor off) suggest that the additional hydrogen signature at 2090 cm^{-1} comes from a heavily hydrogenated region surrounding the nanocrystallites; commonly referred to as the grain boundary region. This identification is supported by FTIR experiments by other groups, which suggest that absorption at higher wavenumbers, in addition to being from clustered Si-H or Si-H_2 in the amorphous phase, could be due to Si-H bonds on the crystallite surface [5]. Studies are underway to further elucidate the details of hydrogen diffusion in doped a/nc-Si:H thin films.

Track 2: ***Large-grain re-crystallized Si***

The second track of the project aims at applying the growth model of seeded enhanced crystallization to films with different seed density, as well as studying the effect of furnace annealing on the stress values of the films. In quarter 9, efforts were focused primarily on development of the growth model of seed enhanced crystallization, where the induced silicon nano-

crystal seeds serve as pre-existing nucleation sites, and the growth originating from the seeds can be divided into two stages: the initial grain growth originated from the seeds before adjacent growth fronts meet with each other, and a second stage in which growth fronts collide, and growth can only proceed in the remaining amorphous gaps between grains.

In this quarter, we studied the macroscopic crystallization kinetics, with 200 nm films of varied seed population density deposited on top of Corning glass substrates and annealed at 650 °C under nitrogen flow in a quartz furnace. Crystal grain growth was monitored by the progression of the Raman crystal volume fraction (X_c) which was measured by Raman spectroscopy at regular time intervals. Crystal fractions were subsequently calculated using the technique of Smit et al [6]. Films containing single layers of cubic seeds with seed crystal population densities between 20-90 particles/μm^2 were compared to films of equal thickness containing no seeds.

As seen in Figure 4, the introduction of the seeds provides a substantial enhancement of crystallization over non-seeded films with full elimination of the amorphous incubation time. By increasing the seed density from 1 particle/μm^2 to 20 particle/μm^2, interestingly the crystallization rate decreases. As re-iterated in past quarters, these results are fortuitously un-expected.

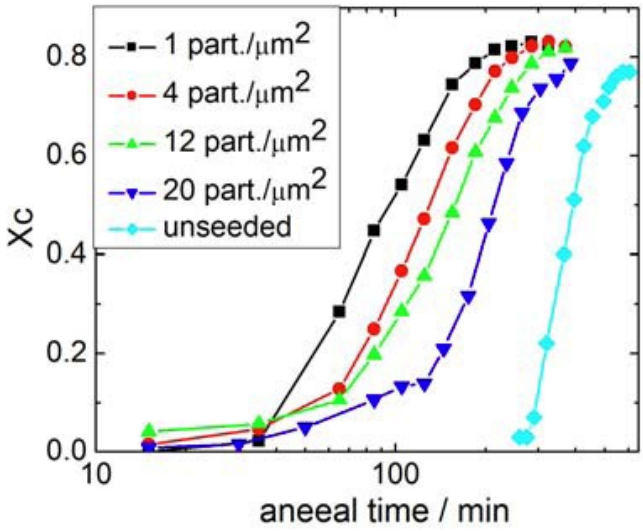

Figure 4: Plot of volume of crystalline fraction as a function of annealing time, for seeded and unseeded films.

Specifically, intuition tells us that sparsely seeded films should produce relatively larger grains, while more heavily seeded structures should crystallize faster on account of having more growth sites. As seen in figure 4, however, an entirely contrasting trend occurs, with more sparsely seeded films crystallizing faster than their more heavily seeded counterparts. By fitting the crystallization curves with the growth model outlined in the previous quarter, a quantitative analysis of the seeded film grain growth rate can be conducted, as seen in Table 1. These values are critical in that they allow estimations to be made of the maximum seed spacing that can be used while still maintaining a grain structure dictated only by seed crystals.

Seed density (part./ μm^2)	Grain growth rate Vg (nm/min)	
	Stage 1	Stage 2
1	4.15	4.46
4	2.92	3.57
12	2.44	2.87
20	1.49	3.01

Table 1: Growth parameters of the seeded films fit with the proposed growth model.

For instance, since native nucleation of our purely amorphous films occurs after an incubation period of approximately 250 min at this temperature, a sample seeded at 1 particle per square micron will be able to grow to a maximum size of 1 micron before the emergence of native grain clusters. As can be seen in figure 5, a 1 micron thick film with these grain dimensions would serve as a very effective absorber layer in a PIN junction device. As figure 5 illustrates, a comparison of the most successful annealed, polysilicon based devices show that open circuit voltage (the primary metric by which absorber layer quality is compared) depends little on average grain diameter, in fact the highest performing device has only a 1 micron average grain diameter. Rather, recent studies show that the ability to maintain high crystalline quality and electronic transport in the film thickness dimension is more crucial to film performance [7]. Studies measuring the electronic transport in the thickness dimension of the seeded structure are currently underway in quarter 11.

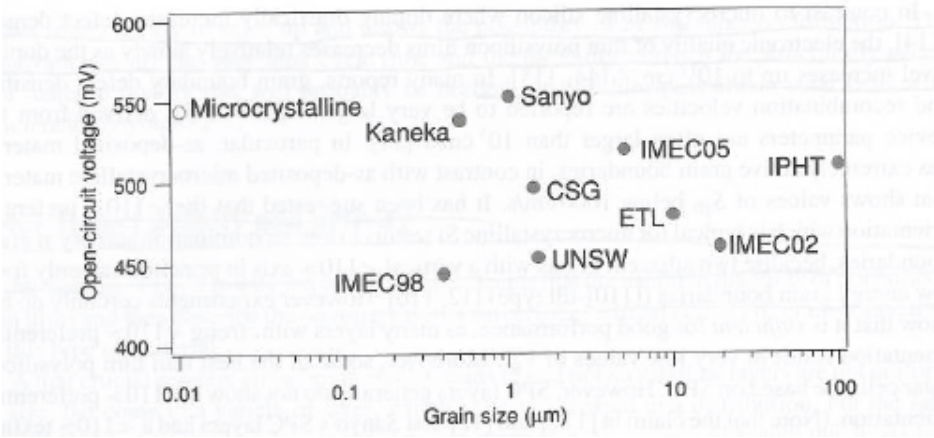

Figure 5. Compilation of the best open circuit voltage values obtained with thin polysilicon solar cells, plotted as a function of grain size [8].

Furthermore, grain orientation is argued to be important as well, with many suggesting an ideal structure to consist of grains having (110) or (220) directions normal to the film surface, since these grains form lower-angle grain boundaries. This has traditionally proven difficult for most of the methods which produced the devices of figure 5, mainly because they rely heavily on

crystallization mechanisms which default to other orientations; typically distributions of various orientations.

Due to our unique ability to vary seed crystal shape and thus surface orientation, however, our seeded structures carry unique potential for grain orientation control [9-12]. X-ray diffraction studies are currently underway in quarter 11 to determine the orientations yielded by various seeded structures.

In further evaluating the viability of our seeded structures relative to other methods, it is also beneficial to compare annealing requirements. Since different methods utilize different temperatures, times, and film sizes, a basic comparison can be made using the metric developed by Nguyen *et al.* [13], defined as the "annealing factor" , given as:

$$A_F = \frac{(T \times t)}{d}$$

where T is the annealing temperature in Celsius, t is the annealing time in minutes, and d is the thickness of the film in nanometers. Lower annealing factors indicate a more desirable process. A comparison of annealing factors between seeded film structures, the top performing devices shown in figure 5, and other popular crystallization methods can be seen in figure 6. Since maintaining a low deposition temperature is also crucial to low cost processing; allowing cheaper substrates on top of reducing overall thermal budget, the annealing factors in figure 6 are plotted with respect to deposition temperature. This illustrates the common sacrifice of low cost polysilicon production, wherein lowering the thermal budget of annealing, usually comes at the expense of a deposition process requiring relatively high temperatures. Subsequently, more optimal processes should reside in the lower left corner of the graph, where it can be seen that our seeded film structures exhibit a clear advantage over even the highest performing absorber layers. It should also be noted that the data points coming closest in performance, method 4 utilizes an Aluminum induced crystallization technique known for leaving metallic impurities in the resulting grain structures, which have been shown to reduce cell performance drastically.

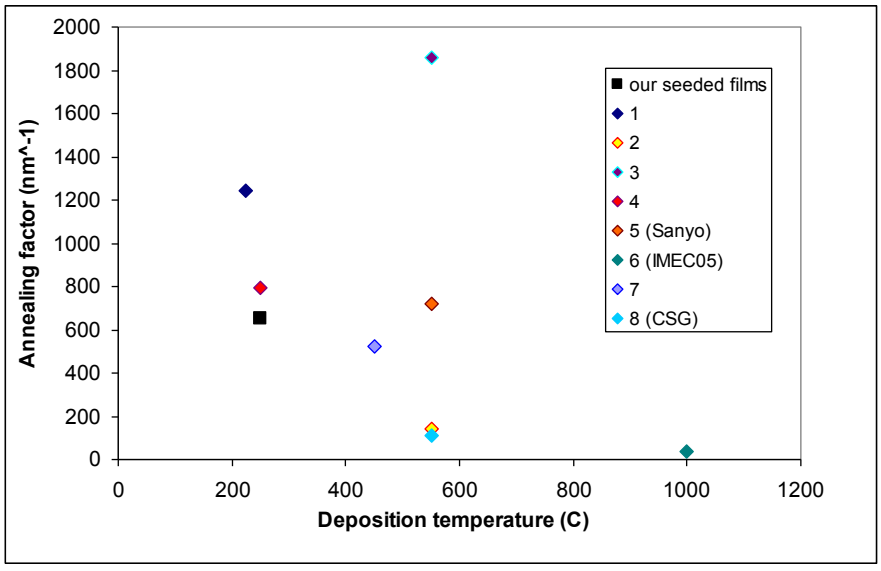

Figure 6. Plot of annealing factor vs. film deposition temperature for various literature and top performing techniques of polysilicon fabrication. Most optimal processes should occupy regions closest to the origin. Process values taken as follows: 1-[14],2-[15],3-[13],4-[16],5-[17],6-[18],7-[19],8-[20].

Since our seeded films consist only of silicon-based components, impurity levels are negligible.

Ultimately, progress in quarter 10 has effectively developed a means for quantifying the grain growth rate in our seeded film structures, which has in-turn, enabled preliminary assessments to be made on the viability of our films relative to the most popular and top-performing methods. Furthermore, efforts to determine the relevant electronic quality are underway in concert with investigating ways to further exploit the crystal synthesis technologies unique to our group to control film properties such as grain orientation, which have yet to be manipulated reproducibly in polysilicon literature.

References:

[1] J. Kakalios and R. A. Street, *Phys.Rev.B* **34**, 6014 (1986).

[2] J. Kakalios, R. A. Street and W. B. Jackson, *Phys. Rev. Lett.* **59**, 1037 (1987).

[3] J. Kakalios and W. B. Jackson, in Amorphous Silicon and Related Materials, edited by H. Fritzsche (World Scientific Publishing Company, 1988), pp. 207.

[4] Y. Adjallah, C. Anderson, U. Kortshagen and J. Kakalios, *J. Appl. Phys.* **107**, 043704 (2010).

[5] D. C. Marra, E. A. Edelberg, R. L. Naone and E. S. Aydil, *J. Vac. Sci. Technol. A* **16**, 3199 (1998); V. A. Burrows, Y. J. Chabal, G. S. Higashi, K. Raghavachari and S. B. Christman, *Appl. Phys. Lett.* **53**, 998 (1988).

[6] C. Smit, R. A. C. M. M. van Swaaij, H. Donker, A. M. H. N. Petit, W. M. M. Kessels, and M. C. M. van de Sanden, Journal Of Applied Physics **94**, 3582-3588 (2003).

[7] S. Gall, J. Schneider, J. Klein, K. Hubener, M. Muske, B. Rau, E. Conrad, I. Sieber, K. Petter, K. Lips, M. Stoger-Pollach, P. Schattschneider, W. Fuhs 2006, "Large-grained polycrystalline silicon on glass for thin-film solar cells"*, Thin Solid Films.* **511-512**, 7-14.

[8] J Poortmans and V Arkhipov, "Thin Film Solar Cells: fabrication, characterization, and applications", *Wiley Publishing,* 2006.

[9] Kortshagen U and Bhandarkar U 1999 "Modeling of particulate coagulation in low pressure plasmas", *Phys. Rev.* E **60** 887.

[10] Mangolini L and Kortshagen U 2009 "Selective nanoparticle heating: another form of nonequilibrium in dusty plasmas", *Phys. Rev.* E **79** 026405.

[11] X D Pi, R W Liptak, J Deneen Nowak, N P Wells, C B Carter, S A Campbell and U Kortshagen 2008, "Air-stable full-visible-spectrum emission from silicon nanocrystals sunthesized by an all-gas-phase plasma approach", *Nanotechnology* **19** 245603.

[12] Bapat A, Gatti M, Yong-Ping D, Campbell S A and Kortshagen U 2006, "A plasma process for the synthesis of cubic-shaped silicon nanocrystals for nanoelectronic devices", *J. Applied Physics,* **40** 2247-2257.

[13] Thanh Nga Nguyen, Van Duy Nguyen, Sungwook Jung, and Junsin Yi 2009, Applied Surface Science **255**, 8252-8256.

[14] R Garcia, M Estrada, A Cerdeira 2003, "Effects of impurity concentration, hydrogen plasma process, and crystallization temperature on poly-crystalline films obtained from PECVD a-Si:H layers"*, Phys. Rev. Lett.* **43**, 1281-1287.

[15] T. Mohammed-Brahim, K. Kis-Sion, D. Briand, M. Sarret, O. Bonnaud, J.P. Kleider, C. Longeaud, B. Lambert 1998, "From amorphous to polycrystalline thin films: dependence on annealing time of structural and electronic properties", *J. Non-Cryst. Solids.* **227-230**, 962-966.

[16] Ö. Tüzün, A. Slaoui, S. Roques, A. Focsa, F. Jomard, D. Ballutaud 2009, "Solid phase epitaxy on N-type polysilicon films formed by aluminium induced crystallization of amorphous silicon", *Thin Solid Films.* **517**, 6358-6363.

[17] T Baba, T Matsuyama, T Sawada, T Takahama, K Wakisaka, S Tsuda 1995, "High-quality polycrystalline silicon thin film prepared by a solid phase crystallization method", *Mat. Res. Soc. Symp. Proc.* **358**, 895-901.

[18] I Gordon, L Carnel, D Van Gestel, G Beaucarne, J Poortmans 2007, "Fabrication and characterization of highly efficient thin-film polycrystalline-silicon solar cells based on aluminium-induced crystallization", *Thin Solid Films.* **516**, 6984-6988.

[19] D. Toet, B. Koopmans, P. V. Santos, R. B. Bergmann, and B. Richards 1996, "Growth of polycrystalline silicon on glass by selective laser-induced nucleation", *Appl. Phys. Lett.* **69** (24), 3719-3721.

[20] D.H. Neuhaus, R. Bardos, L. Feitknecht, T. Puzzer, M.J. Keevers, and A.G. Aberle 2000, *IEEE* 0-7803-5772-8/00, 65-68.